Memoirs of the Faculty of Engineering, Nagoya University
Vol. 39, No.2 (1987) —Research Report—

COMPUTATION OF HYPERVELOCITY THREE-DIMENSIONAL REACTING FLOWS

K. V. REDDY and TOSHI FUJIWARA

Department of Aeronautical Engineering

(Received October 26, 1987)

Abstract

A hybrid computational procedure is developed to compute three-dimensional, hypersonic and chemically reacting flowfields around reentry vehicles. The medium is assumed to be a multi-component mixture of thermally perfect but calorically imperfect gases. As the governing equations are integrated between the peripheral bow shock and body surface using an implicit finite-difference scheme, stiffness in species conservation equations did not pose any difficulty. Results for two-dimensional and three-dimensional flows show that chemical reactions render the bow shock close to the body.

1. Introduction

It is well known that air in non-equilibrium flows undergoes vibrational excitation, dissociation, and ionisation. These chemical phenomena absorb energy, change compressibility and cause temperature to fall and density to rise. At low altitudes, where the air density is high, these chemical phenomena quickly reach thermodynamic equilibrium and the nonequilibrium state appears as a transient phenomenon. At high altitudes, where the density is low, chemical states do not necessarily reach equilibrium and the non-equilibrium state appears as a steady state phenomenon. If a space shuttle chooses a high-altitude trajectory (1), a considerable period of nonequilibrium flow occurs during atmospheric reentry. This leads to a renewed interest in flows with finite-rate chemical reactions, that is, non-equilibrium flows generated by reentry vehicles.

Computing a non-equilibrium reacting flow around a reentry body of three-dimension is considerably difficult. In such a flow, the dynamic behavior of the flow is affected significantly by chemical reactions, hence the momentum equations must be solved simultaneously with the species conservation equations governing the chemical phenomena (2). The purpose of this work is to develop a versatile

code, which can handle stiff problems associated with fast reactions, by extending the implicit hybrid numerical scheme developed for real gases by the same authors (3).

2. Mathematical Formulation

Formulation of a fluid dynamics problem including chemical reactions depends on general concepts from the three areas: Chemical kinetics, thermodynamics and gas dynamics.

(a) Chemical kinetics: Suppose that a mixture consists of N chemical species undergoing m elementary reactions. The n-th reaction may be written as

$$\underbrace{\sum_{l=1}^{N} \nu_l^{(n)'} A_l}_{\text{reactants}} \underset{k_r^{(n)}}{\overset{k_f^{(n)}}{\rightleftarrows}} \underbrace{\sum_{l=1}^{N} \nu_l^{(n)''} A_l}_{\text{products}}, \tag{1}$$

where $\nu_l^{(n)'}$ and $\nu_l^{(n)''}$ are the stoichiometric coefficients of reactants and products, respectively, giving the number of moles participating in that particular reaction, A_l denotes the chemical symbol of the l th species, $k_f^{(n)}$ and $k_r^{(n)}$ are the forward and reverse specific reaction rate constants for n-th reaction. Progress in the forward direction of the n-th reaction is expressed as

$$R^{(n)} = k_f^{(n)} \prod_{l=1}^{N} [C_l]^{\nu_l^{(n)'}} - k_r^{(n)} \prod_{l=1}^{N} [C_l]^{\nu_l^{(n)''}}, \tag{2}$$

where $[C_l] = Y_l/M_l$ is the molar concentration, $Y_l = \rho_l/\rho$ the mass fraction and M_l the molecular weight of l-th species. Since n-th reaction yields $\nu_l^{(n)'} - \nu_l^{(n)''}$ moles of A_l, the corresponding mass rate of production of A_l is

$$\dot{W}_l^{(n)} = M_l [\nu_l^{(n)''} - \nu_l^{(n)'}] R^{(n)}. \tag{3}$$

It follows that the net mass rate of production of A_l in an m-elementary-reactions system is

$$\dot{W}_l = \sum_{n=1}^{m} \dot{W}_l^{(n)}. \tag{4}$$

Combining Eqs. (2) to (4), we have

$$\dot{W}_l = \sum_{n=1}^{m} M_l [\nu_l^{(n)''} - \nu_l^{(n)'}] \left[k_f^{(n)} \prod_{l=1}^{N} [C_l]^{\nu_l^{(n)'}} - k_r^{(n)} \prod_{l=1}^{N} [C_l]^{\nu_l^{(n)''}} \right]. \tag{5}$$

If n-th reaction is in equilibrium, it follows from Eq. (2) that

$$K_c^{(n)} = \frac{k_f^{(n)}}{k_r^{(n)}} = \prod_{l=1}^{N} [C_l]^{(\nu_l^{(n)''} - \nu_l^{(n)'})}, \tag{6}$$

which is the chemical equilibrium condition of the n-th reaction and $K_c^{(n)}$ is the corresponding equilibrium constant. From statistical thermodynamic principles, $K_c^{(n)}$ can be expressed as a function of temperature.

The chemical kinetics of air dissociation generally involves the interplay of

about 20 different chemical components entering into over 100 elementary reactions. Fortunately, most of these reactions involve only chemically minor species and therefore only 5 species O_2, N_2, N, O, and NO participate into the five significant reactions:

$$O_2 + M \underset{k_r^{(1)}}{\overset{k_f^{(1)}}{\rightleftarrows}} O + O + M, \tag{7}$$

$$N_2 + M \underset{k_r^{(2)}}{\overset{k_f^{(2)}}{\rightleftarrows}} N + N + M, \tag{8}$$

$$NO + M \underset{k_r^{(3)}}{\overset{k_f^{(3)}}{\rightleftarrows}} N + O + M, \tag{9}$$

$$O + N_2 \underset{k_r^{(4)}}{\overset{k_f^{(4)}}{\rightleftarrows}} NO + N, \tag{10}$$

$$NO + O \underset{k_r^{(5)}}{\overset{k_f^{(5)}}{\rightleftarrows}} N + O_2, \tag{11}$$

where M is an any third molecule serving to absorb excess energy released during the collision process.

Chemical source functions for these five species can be written, following Eq. (1), as

$$\dot{W}_{O_2} = M_{O_2}\frac{dC_{O_2}}{dt} = M_{O_2}[-C_{O_2}C_M k_f^{(1)} + C_{O_2}^2 C_M k_r^{(1)} + C_{NO}C_O k_f^{(5)} - C_N C_{O_2} k_r^{(5)}], \tag{12}$$

$$\dot{W}_{N_2} = M_{N_2}\frac{dC_{N_2}}{dt} = M_{N_2}[-C_{N_2}C_M k_f^{(2)} + C_N^2 C_M k_r^{(2)} - C_O C_{N_2} k_f^{(4)} + C_{NO}C_N k_r^{(n)}], \tag{13}$$

$$\begin{aligned}\dot{W}_N = M_N\frac{dC_N}{dt} = M_N[&2C_{N_2}C_M k_f^{(2)} - 2C_N^2 C_M k_r^{(2)} + C_{NO}C_M k_f^{(3)} - C_N C_O C_M k_r^{(3)} \\ &+ C_O C_{N_2} k_f^{(4)} - C_{NO}C_N k_r^{(4)} + C_{NO}C_O k_f^{(5)} - C_N C_{O_2} k_r^{(5)}],\end{aligned} \tag{14}$$

$$\begin{aligned}\dot{W}_O = M_O\frac{dC_O}{dt} = M_O[&2C_{O_2}C_M k_f^{(1)} - 2C_O^2 C_M k_r^{(1)} + C_{NO}C_M k_f^{(3)} - C_N C_O C_M k_r^{(3)} \\ &- C_O C_{N_2} k_f^{(4)} + C_{NO}C_N k_r^{(4)} - C_{NO}C_O k_f^{(5)} + C_N C_{O_2} k_r^{(5)}],\end{aligned} \tag{15}$$

$$\begin{aligned}\dot{W}_{NO} = M_{NO}\frac{dC_{NO}}{dt} = M_{NO}[&-C_{NO}C_M k_f^{(3)} + C_N C_O C_M k_r^{(3)} + C_O C_{N_2} k_f^{(4)} - C_{NO}C_N k_r^{(4)} \\ &- C_{NO}C_O k_f^{(5)} + C_N C_{O_2} k_r^{(5)}].\end{aligned} \tag{16}$$

In Reactions (7) through (11) M can be any molecule other than the two reacting molecules that are involved in the collision process. In a certain reaction, the reaction rate constant depends on the molecules that serve as M. By assuming no priority among the molecules representing M, the probability of a particular species to act as the third body M can be proportional to its number density. With this,

the terms $C_M k_f^{(n)}$ and $C_M k_r^{(n)}$ appearing in Eqs. (12) through (16) can be replaced by the summation

$$C_M k_f^{(n)} = \sum_{l=1}^{5} C_l k_{f,l}^{(n)} \quad \text{and} \quad C_M k_r^{(n)} = \sum_{l=1}^{5} C_l k_{r,l}^{(n)}, \tag{17}$$

where $k_{f,l}^{(n)}$ and $k_{r,l}^{(n)}$ represent the specific forward and backward reaction rates of n-th reaction when l-th species is acting as the third body.

Determination of reaction rate constants: The reaction rate is a function of temperature expressed in a modified Arrhenius form as

$$k_f^{(n)} = S_n T^{\beta} \mathrm{Exp}\left(-\frac{E_a}{T}\right), \tag{18}$$

$$k_r^{(n)} = k_f^{(n)} / K_c^{(n)}, \tag{19}$$

where the equilibrium constant $K_c^{(n)}$ is again a function of temperature only. Although from the available spectroscopic data one can evaluate $K_c^{(n)}$ for a given reaction at a given temperature, a unique correlation between $K_c^{(n)}$ and T is hardly available. Park (4) fitted the natural logarithm of computed $K_c^{(n)}$ values using the following expression in $z = 10000/T$:

$$K_c(T) = \exp(A_1 + A_2 \ln(z) + A_3 z + A_4 z^2 + A_5 z^3). \tag{20}$$

The constants in this expression are evaluated using spectroscopic data at temperatures of 1000, 2000, 4000, 8000 and 16000°K. In the present work the same expression is used to calculate equilibrium constants. The coefficients A_1 through A_5 are listed in Table 1, along with the constants appearing in the Arrhenius equation (18).

Table 1. The Constants Appearing in Eqs. (18) and (20) for Different Reactions

Reaction		S_n	β	E_a	A_1	A_2	A_3	A_4	A_5
$O_2+M \rightleftarrows O+O+M$	$M=O_2$	2.75E19	-1.0	59500	2.855	0.988	-6.181	-0.023	-0.001
	$M=N_2$	2.75E19							
	$M=O$	8.25E19							
	$M=N$	8.25E19							
	$M=NO$	2.75E19							
$N_2+M \rightleftarrows N+N+M$	$M=O_2$	3.70E21	-1.6	113200	1.858	-1.325	-9.856	-0.174	0.008
	$M=N_2$	3.70E21							
	$M=O$	1.11E21							
	$M=N$	1.11E21							
	$M=NO$	3.70E21							
$NO+M \rightleftarrows N+O+M$	$M=O_2$	2.30E17	-0.5	75500	0.792	-0.492	-6.761	-0.091	0.004
	$M=N_2$	2.30E17							
	$M=O$	4.60E17							
	$M=N$	4.60E17							
	$M=NO$	2.30E17							
$O+N_2 \rightleftarrows N+NO$		3.18E13	0.1	37700	1.066	-0.833	-3.095	-0.084	0.004
$NO+O \rightleftarrows N+O_2$		2.16E08	1.29	19220	-2.063	-1.480	-0.580	-0.114	0.005

(*b*) *Thermodynamics*: The thermodynamic state of a gaseous mixture of N components among which chemical reactions may occur is completely specified by N+2 independent variables. A study of thermodynamics (5) shows that other relations can be found that define a new set of variables, each as a function of the N+2 independent variables. A fundamental thermodynamic equation is any equation relating these new variables to the N+2 independent ones. For example, the fundamental thermodynamic equation

$$p=p(\rho,\ e,\ Y_l), \tag{21}$$

relates the pressure p to the N+2 independent variables; the density ρ, specific internal energy e and mass fraction Y_l of N species. Assuming that the gas under consideration is in thermal equilibrium and all the chemical species are thermally perfect gases, an explicit form of the equation of state (21) can be obtained in a dimensionless form as

$$p=\sum_{l=1}^{5} Y_l h_l+\frac{1}{2}\rho(u^2+v^2+w^2)-e, \tag{22}$$

where h_l is the specific enthalpy of l-th species. The thermodynamic properties h_l and c_p for all the five species are obtained from JANAF Tables (6). In addition an expression for the temperature T can be derived as

$$T=p/(\rho\overline{R}) \text{ where } \overline{R}=R_0\sum_{l=1}^{5}(Y_l/M_l). \tag{23}$$

(*c*) *Gasdynamics*: The flow condition is completely specified by the requirement that mass, momentum and energy are conserved throughout the flowfield and along its time and space boundaries. Therefore the complete formulation of a reacting gas mixture of N species is made of N+5 coupled non-linear partial differential equations of continum mechanics; the mass of N species, momentum and energy conservations and equation of state. The solution of these coupled equations in N+5 variables yields the composition, density, velocity, and thermal state of the system at every point. A complete system of equations that describe the adiabatic and non-diffusive flow of a mixture of reacting gases in chemical non-equilibrium can be written in a conservation law form in a ξ, η, ζ and τ general moving coordinate system (Fig. 1) as

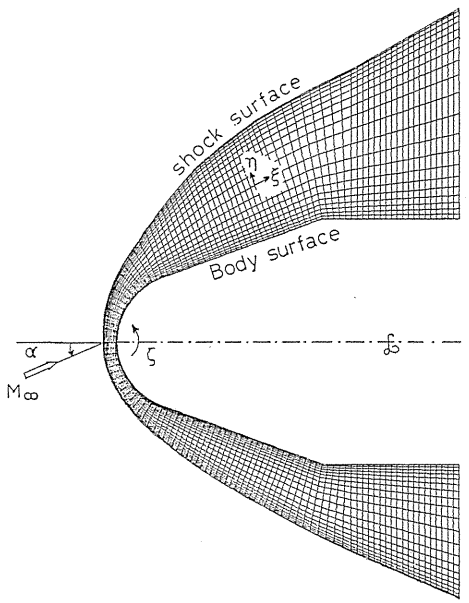

Fig. 1. Body Geometry and Moving Grid System.

$$\frac{\partial\hat{q}}{\partial\tau}+\frac{\partial\hat{E}}{\partial\xi}+\frac{\partial\hat{F}}{\partial\eta}+\frac{\partial\hat{G}}{\partial\zeta}+\hat{H}=0, \tag{24}$$

where
$$\hat{q}=J^{-1}\begin{pmatrix}\rho_1\\ \rho_2\\ \rho_3\\ \rho_4\\ \rho_5\\ \rho u\\ \rho v\\ \rho w\\ e\end{pmatrix},\quad \hat{E}=J^{-1}\begin{pmatrix}\rho_1 U\\ \rho_2 U\\ \rho_3 U\\ \rho_4 U\\ \rho_5 U\\ \rho uU+\hat{\xi}_x p\\ \rho vU+\hat{\xi}_y p\\ \rho wU+\hat{\xi}_z p\\ (e+p)U-\hat{\xi}_t p\end{pmatrix},$$

$$\hat{F}=J^{-1}\begin{pmatrix}\rho_1 V\\ \rho_2 V\\ \rho_3 V\\ \rho_4 V\\ \rho_5 V\\ \rho uV+\eta_x p\\ \rho vV+\eta_y p\\ \rho wV+\eta_z p\\ (e+p)V-\eta_t p\end{pmatrix},\quad \hat{G}=J^{-1}\begin{pmatrix}\rho_1 W\\ \rho_2 W\\ \rho_3 W\\ \rho_4 W\\ \rho_5 W\\ \rho uW+\zeta_x p\\ \rho vW+\zeta_y p\\ \rho wW+\zeta_z p\\ (e+p)W-\zeta_t p\end{pmatrix}\quad\text{and}\quad \hat{H}=J^{-1}\begin{pmatrix}-c\dot{W}_{O_2}\\ -c\dot{W}_{N_2}\\ -c\dot{W}_{N}\\ -c\dot{W}_{O}\\ -c\dot{W}_{NO}\\ 0\\ 0\\ 0\\ 0\end{pmatrix},$$

and the contravariant velocities are given by

$$U=\hat{\xi}_t+\hat{\xi}_x u+\hat{\xi}_y v+\hat{\xi}_z w,$$
$$V=\eta_t+\eta_x u+\eta_y v+\eta_z w,$$
$$W=\zeta_t+\zeta_x u+\zeta_y v+\zeta_z w,$$

and $c=1/\rho_\infty a_\infty^2$ and all the other variables are defined in Ref. 3. In the above equation, the flow variables are non-dimensionalized as

$$x,\ y,\ z=\frac{x,\ y,\ z}{L^*},\quad \rho=\frac{\rho}{\rho_\infty},\quad p=\frac{p}{\rho_\infty a_\infty^2},\quad e=\frac{e}{\rho_\infty a_\infty^2},$$

$$u,\ v,\ w=\frac{u,\ v,\ w}{a_\infty},\quad h=\frac{h}{a_\infty^2}\quad\text{and}\quad t=\frac{a_\infty}{L^*}\tau,$$

where L^* is a reference length.

3. Numerical Scheme

The differential form of governing equations given by Eq. (24) is replaced by the non-iterative approximate factorization implicit scheme of Beam and Warming (7). The scheme can be written as

$$[I+\Delta\tau\,\delta_\xi\hat{A}^n-\Delta\tau\,D_i|_\xi][I+\Delta\tau\,\delta_\eta\hat{B}^n-\Delta\tau\,D_i|_\eta][I+\Delta\tau\,\delta_\zeta\hat{C}^n-\Delta\tau\,D_i|_\zeta]\Delta\hat{q}^n$$
$$=-\Delta\tau(\delta_\xi\hat{E}^n+\delta_\eta\hat{F}^n+\delta_\zeta\hat{G}^n+\hat{H}+D_e\hat{q}^n), \tag{25}$$

where $\hat{A}$, $\hat{B}$ and $\hat{C}$ are the Jacobian matrices and are given in Appendix. δ_ξ, δ_η and δ_ζ are three point central differential operators. The numerical dissipative terms denoted as D_i and D_e are given in Ref. 8.

4. Boundary Conditions

A bow shock in the present formulation is treated as a sharp shock and the computational domain is bounded between the peripheral bow shock and the body surface. The peripheral shock is moved along all the fixed radial lines at the shock velocities $\tilde{W}_s$ after integrating the difference equation (25) over one time step. The floating grid system formed between the moving peripheral shock and the body is generated algebraically (3), such that grid points are clustered near the bow shock and body. The shock velocities $\tilde{W}_s$ are calculated using the pressure p_2 which is extrapolated from the field points, and the Rankine-Hugoniot relations for the moving discontinuity which are given as

$$h_2=h_\infty+0.5(p_2-p_\infty)\left(\frac{1}{\rho_2}+\frac{1}{\rho_\infty}\right), \tag{26}$$

$$\lambda_{\text{shock}}=\left[(p_2-p_\infty)\left(\frac{1}{\rho_\infty}-\frac{1}{\rho_2}\right)\right]^{1/2}-V_{n_\infty}, \tag{27}$$

where λ_{shock} is the shock velocity in the outward normal direction. The frozen shock conditions are explicitly imposed in the formulation by allowing no reactions across the peripheral shock wave. Hence the densities ρ_l behind the shock are calculated from the density behind the shock

$$\left.\frac{\rho_l}{\rho}\right|_2=\left.\frac{\rho_l}{\rho}\right|_\infty, \tag{28}$$

$$\text{i.e.}\quad \rho_l|_2=\left.\frac{\rho_l}{\rho}\right|_\infty\cdot\rho|_2. \tag{29}$$

Using these relations Eqs. (26) and (27) can be solved for the shock velocity λ_{shock}. The other details on the shock treatment are discussed in Ref. 3. On the wall surface the flow is tangent to the body whereas the insulated wall requires the temperature gradient on the wall to vanish. The pressure on the wall is obtained by integrating the normal momentum equation (9)

$$p_\eta(\eta_x^2+\eta_y^2+\eta_z^2)^{1/2}=(\bar{\xi}_x\eta_x+\bar{\xi}_y\eta_y+\bar{\xi}_z\eta_z)\,p_\xi$$
$$+(\zeta_x\eta_x+\zeta_y\eta_y+\zeta_z\eta_z)\,p_\zeta+(\eta_x^2+\eta_y^2+\eta_z^2)\,p_\eta$$
$$=-\rho U(\eta_x u_\xi+\eta_y v_\xi+\eta_z w_\xi)-\rho W(\eta_x u_\zeta+\eta_y v_\zeta+\eta_z w_\zeta). \tag{30}$$

The density along with species concentration is extrapolated from the corresponding value at the neighboring grid points.

5. Stability and Initial Conditions

If the chemical production terms $\dot{w}$ were identically equal to zero, then the linear stability analysis suggests (10)

$$\Delta\tau^*=\min\left\{\frac{\Delta\bar{\xi}}{\lambda_{\max}},\ \frac{\Delta\eta}{\mu_{\max}},\ \frac{\Delta\zeta}{\theta_{\max}}\right\}, \tag{31}$$

where $\lambda_{\max}$, $\mu_{\max}$ and $\theta_{\max}$ are the eigenvalues of the matrices $\hat{A}$, $\hat{B}$ and $\hat{C}$, respectively. Although the production term $\dot{w}$ is too complex for a stability criterion on $\Delta\tau^*$ to be determined analytically, but an empirical condition can be derived from the consideration of chemical relaxation times. In the present experience, it is found that the relation $\Delta\tau=0.2\Delta\tau^*$ allows a stable integration process. As a CFL value equal to 5 works out well for real gases, a CFL number equal to unity is used throughout reacting flow calculations. The initial data for reacting flow calculations are supplied by the real gas code.

6. Results and Discussions

Numerical calculations are performed for the reacting flow around a rocket nose geometry at different flight speeds and angles of attack. The body configuration is obtained by smoothly joining a sphere head of radius R, a conical cylinder of 20° half angle and a cylinder of radius $1.8R$. The freestream is a mixture of 21 percent oxygen and 79 percent nitrogen. The freestream ambient pressure is 5.5 kg/m^2, while the density $\rho_\infty=0.8728\times10^{-4}$ kg/m^3. The ambient temperature is 218.36 °K. Calculations are made for the Mach numbers equal to 15, 20 and 25. These Mach numbers correspond to the flight velocities 4.45, 5.93 and 7.42 km/sec, respectively.

The computed shock structure and shock standoff distance for a two-dimensional body are presented in Fig. 2 and Table 2. For comparison purpose the solutions obtained for the real gas and perfect gas models are also shown. The shock structure is smooth and due to chemical reactions the peripheral shock is moved very close to the body.

The isothermal lines in the reacting flows over a two-dimensional body at three Mach numbers are shown in Fig. 3. For a Mach number 15, calculations are made on the full body configuration whereas for higher Mach numbers calculations are made only near the front region.

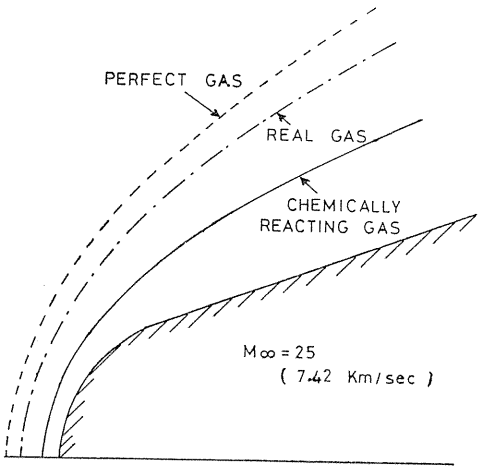

Table 2. Shock Standoff Distances in Perfect Gas, Real Gas and Chemically Reacting Gas Models.

Mach Number	Shock Standoff Distance δ/R		
	Perfect Gas	Real Gas	Chemically Reacting Gas
15.0	0.40294	0.29910	0.20494
20.0	0.38311	0.28289	0.14768
25.0	0.37196	0.27029	0.10952

Fig. 2. Comparison of Shock Structures among Perfect Gas, Real Gas and Chemically Reacting Gas.

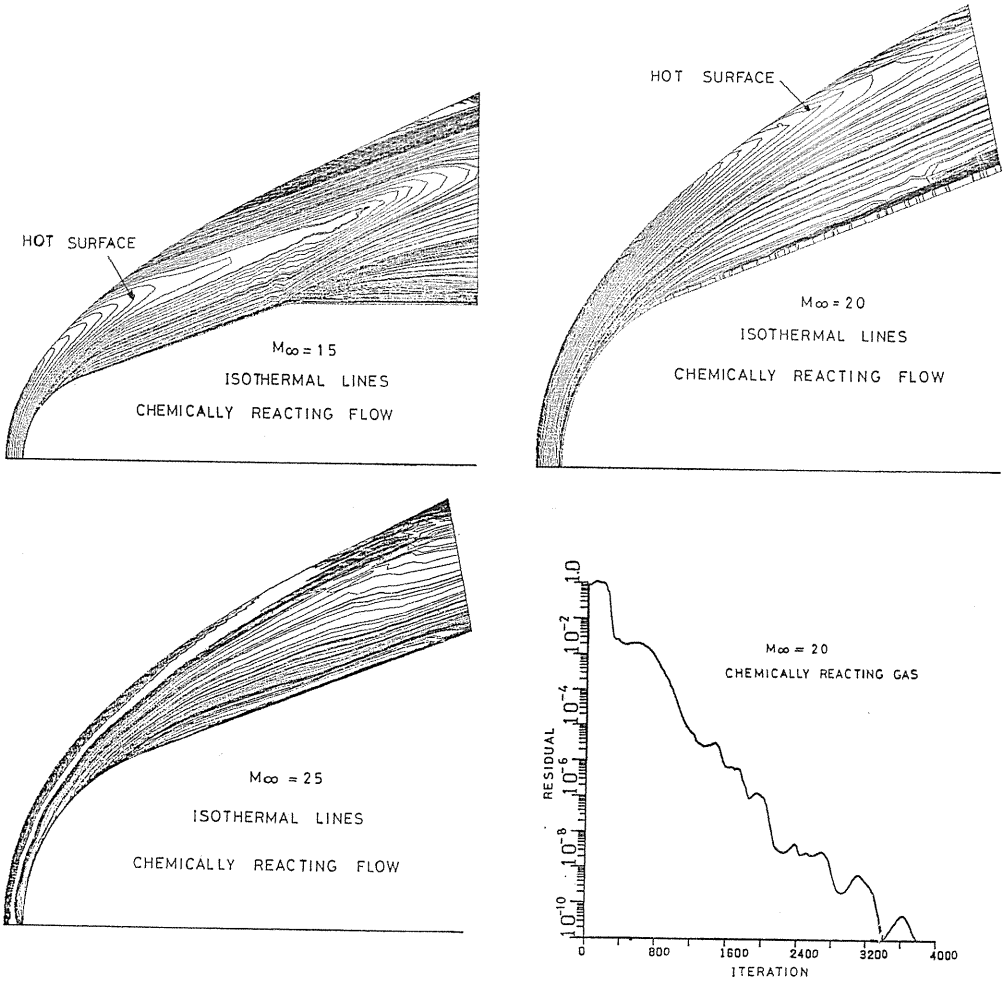

Fig. 3. Isothermal Lines and Convergence History.

As endothermic reactions absorb thermal energy from the system, the local temperature drops where these reactions are significant. If a fluid particle is at a temperature lower than the threshold one, then only a negligibly small number of air molecules will result in reaction products. It is also known that in a real gas flow (3), temperatures monotonically increase from the shock to body surface. Therefore, in the present reaction model, when the temperature reaches a threshold value, reactions occur at a faster rate and thereby the local temperature will drop. This phenomenon results in a hot surface in the flowfield. In other words, the temperature in the flowfield will be maximum at the hot surface and this maximum should correspond to the threshold temperature. In addition this hot surface can be identified as a surface separating the reacted flow from the nonreacted one. This has been clearly observed in the isothermal line plots for the Mach numbers 15 and 20. For these Mach numbers the temperature contours above the hot surface are not different from the real gas solution. For the Mach number 25, the flowfield under consideration is completely reacted and hence no hot surfaces are observed.

The convergence history for the Mach number 20 is shown in Fig. 3, where a 40×40 grid system is used. The total residual is dropped to below 10^{-10} within 4000 iterations, for which a VP-200 computer takes 28.3 min cpu time. The pressure, density, temperature and species concentration distributions along the stagnation line are shown for these three Mach numbers in Fig. 4. At the Mach number 15, more than 70 percent of oxygen has dissociated whereas only a small amount of nitrogen has reacted. Even at this Mach number, the density at the stagnation point is doubled from its non-reacting value and the stagnation temperature has dropped to 3560 K. At the Mach number 20, oxygen molecules immediately after passing through the shock wave dissociate almost completely. However,

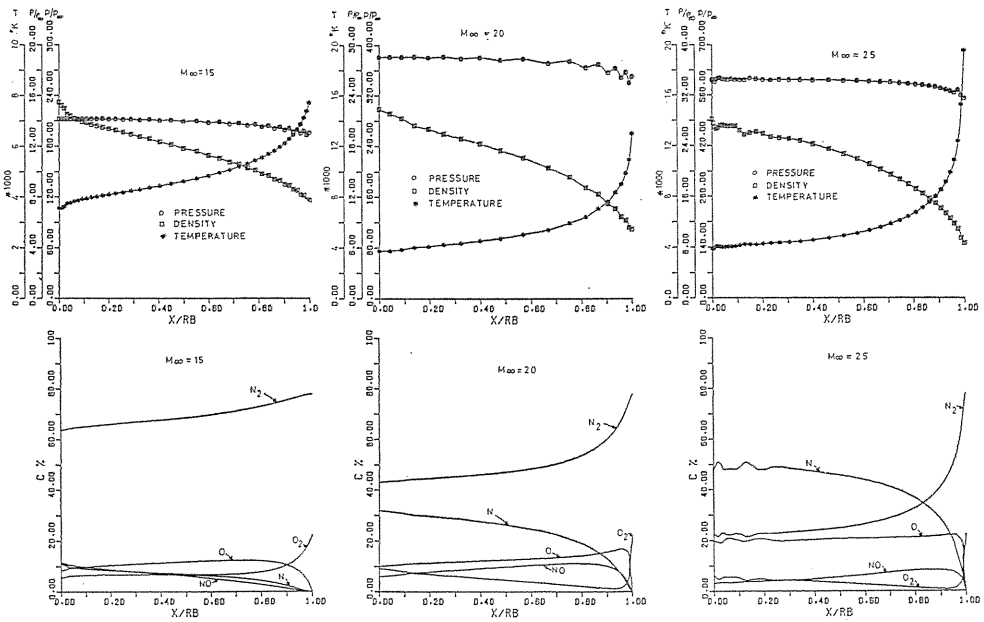

Fig. 4. Pressure, Density, Temperature, and Species Distributions along Stagnation Streamline for M=15, 20 and 25.

when the temperature drops further due to nitrogen dissociation, oxygen molecules reappear in an appreciable amount. When the flight velocity reaches 7.43 km/sec ($M_\infty=25$), numerous oxygen atoms form along the stagnation streamline. Nitric oxide formed behind the shock wave dissociates again near the body. At this Mach number the temperature drops rapidly downstream of the shock. The density at the wall is 3.5 times the value immediately downstream of the shock wave. From

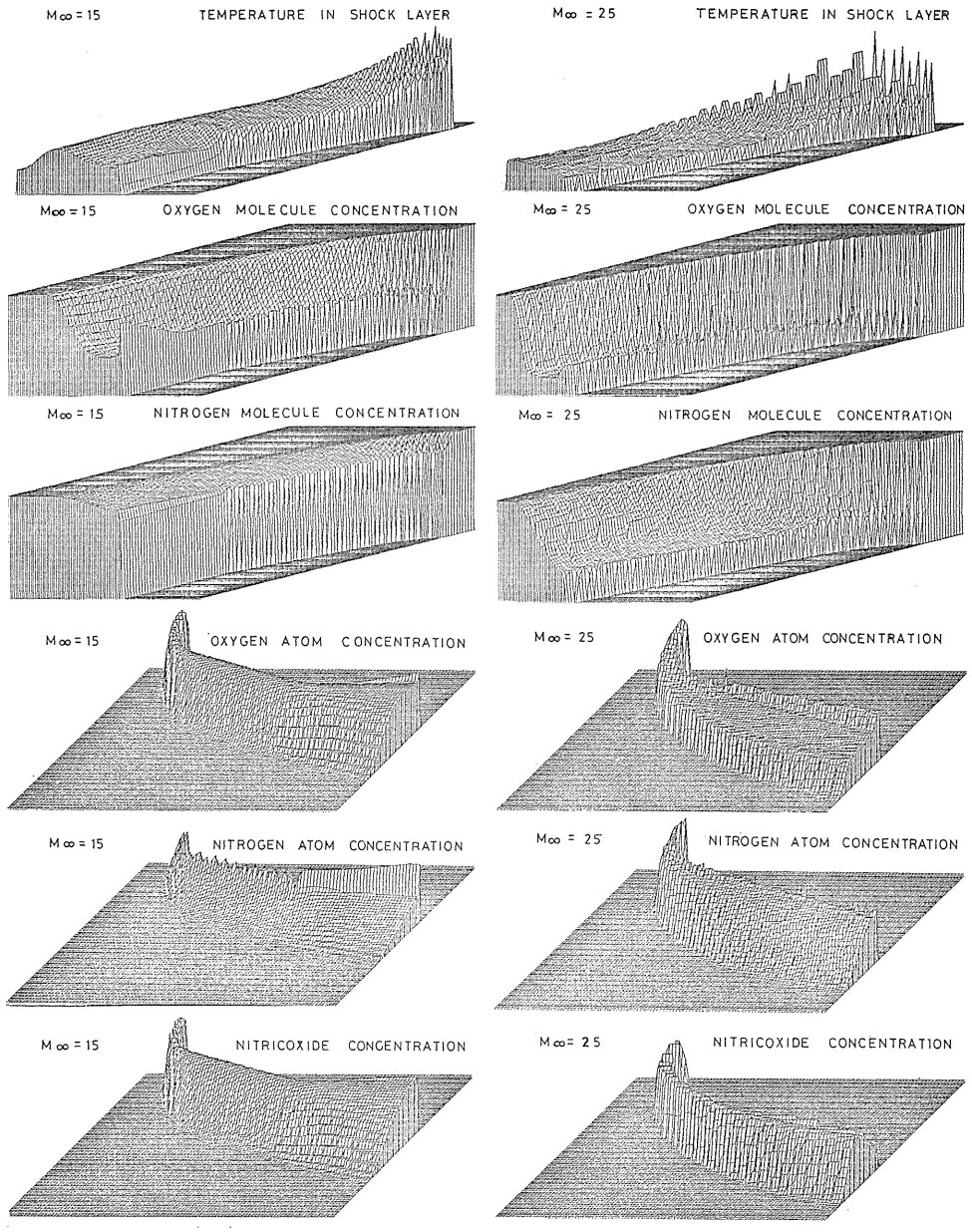

Fig. 5. Flow Visualization.

these calculations it is observed that chemical reactions are very sensitive to the flowfield and, most importantly, nearly all the reactions have completed within a narrow region behind the shock wave. Therefore, in general, shock capturing methods which capture the peripheral bow shock as a diffused shock may change the chemical reaction considerably. The entire flow is visualized in Fig. 5 for the

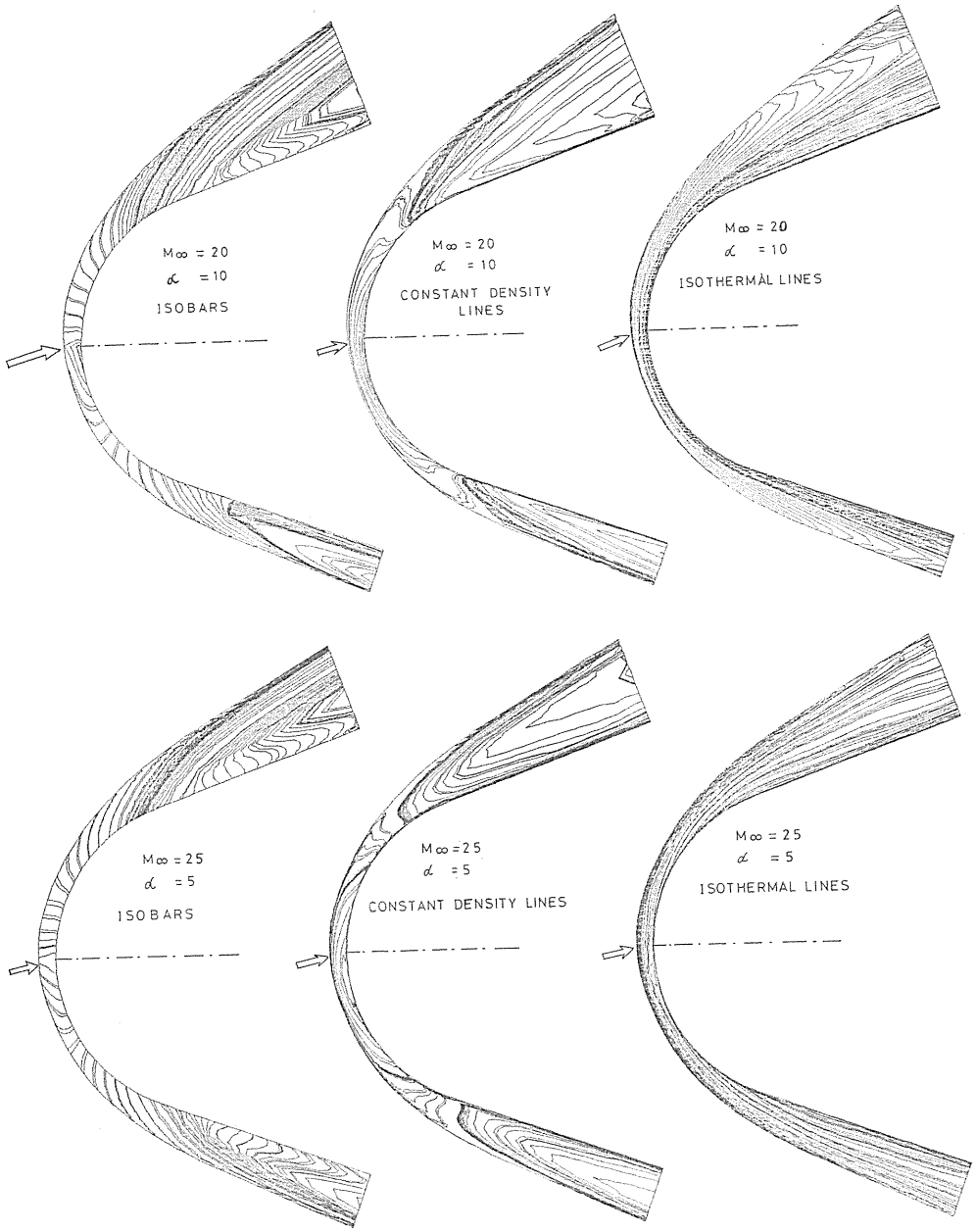

Fig. 6. Isobars, Constant Density and Isothermal Lines in Flows around Axisymmetrics Bodies at Angles of Attack.

Mach numbers 15 and 25. For the Mach number 15, a hot surface can be seen in the temperature plot. The scales are different from one picture to anoother.

For the same ambient flow conditions, reacting flows over the axisymmetric nose portion of a rocket body are computed for the Mach number 20 freestream flow at an angle of attack 10° and for the Mach number 25 at an angle of attack 5°. The results in the form of isobars, constant density lines and isothermal lines are shown in Fig. 6. The calculation is performed over a $40\times30\times20$ grid system. A steady state solution is obtained after 2000 time steps. For each case, a VP-200 computer takes nearly 2 hours cpu time. Hot surfaces are observed in these flows as well. The pressure, density, temperature and species concentration distributions

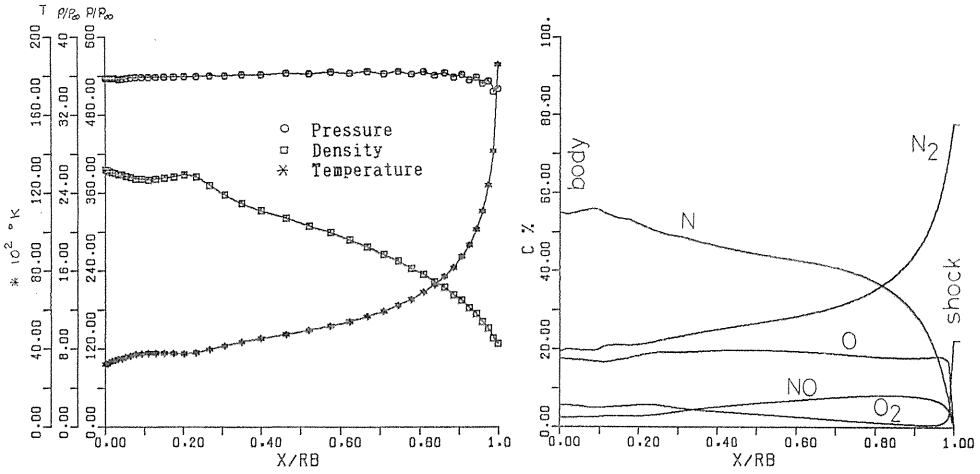

Fig. 7a. Pressure, Density, Temperature and Species Concentrations along an η line ($\xi=0.0$). $M_\infty=25$ and $\alpha=5°$.

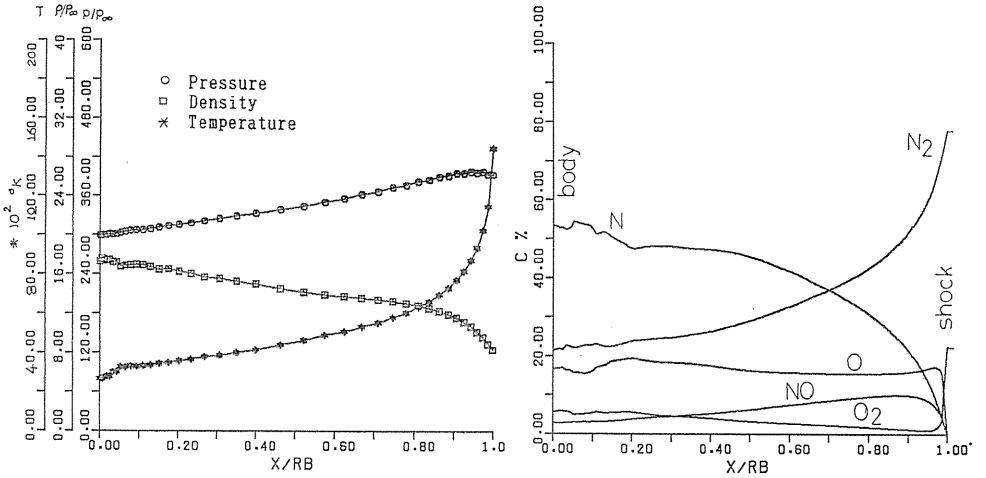

Fig. 7b. Pressure, Density, Temperature, and Species Concentrations along an η line ($\xi=0.785$R, $\zeta=0°$). $M_\infty=25$ and $\alpha=5°$.

along different radial lines are shown in Figs. 7(a) through 7(d) for the Mach number 25 and $\alpha=5°$. Weak oscillations in the flow variables are observed near the body surface. These are due to the insufficient grid spacings near the body. Nitrogen atom concentrations everywhere along the body surface are high and as a result are the dominant species near the wall surface. Far downstream of the stagnation streamline, i.e. at $\xi=2.07R$, oxygen molecules dissociate gradually. At this location the solution is yet to be stabilized. In these problems, since the shock standoff distance is very small, the time step calculated from the stability criterion corresponds to the grid spacing on the stagnation streamline. The flow computed at the far downstream using the same time step converges slowly. A

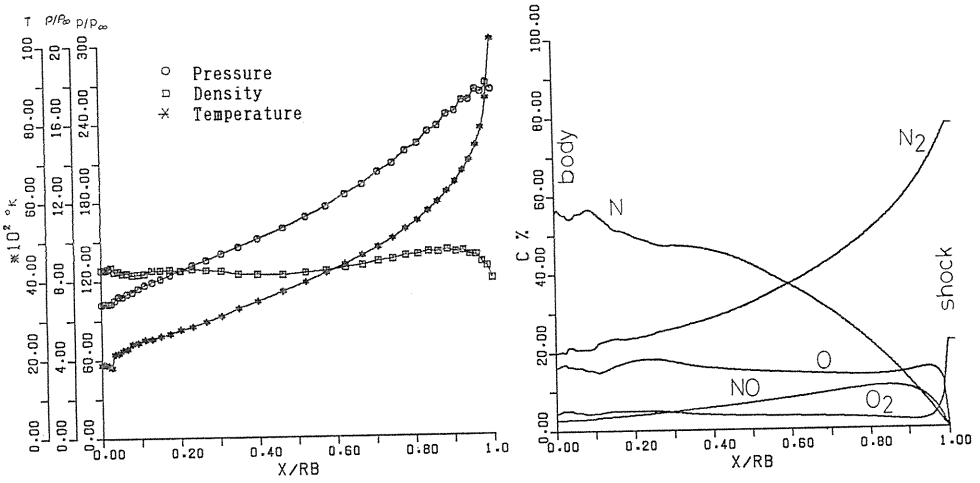

Fig. 7c. Pressure, Density, Temperature, and Species Concentrations along an η line ($\xi=0.785$R, $\zeta=180°$). $M_\infty=25$ and $\alpha=5°$.

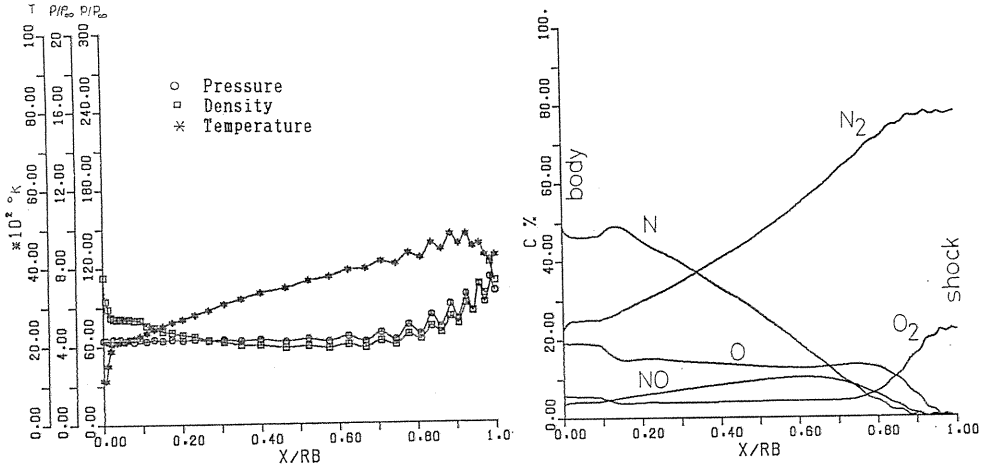

Fig. 7d. Pressure, Density, Temperature, and Species Concentrations along an η line ($\xi=2.07$R, $\zeta=180°$). $M_\infty=25$ and $\alpha=5°$.

variable time step does not seem to work in reacting flow calculations. To avoid such difficulties the production terms in Eq. (25) had better be treated implicitly. Note, however, that this increases computer memory enormously.

7. Conclusions

Reacting flows over two-dimensional and axisymmetric bodies at angles of attack are computed successfully using an implicit hybrid scheme. Large amount of computer time is necessary partly because of the increased number of independent variables and partly due to the severe restrictions on the time step caused by the chemical production terms. A more logical way of increasing the time step is by solving two different sets of governing equations separately: One set of equations are usual ones whereas the other set of governing equations can be written only for chemical species conservation. The latter set of equations can be solved at a smaller time step until the solution catches up with the time step allowed for the complete governing equations (time step for the complete governing equations is calculated by making the production terms identical to zero). Then the complete governing equations can be integrated at a larger time step. Such an investigation is currently going on.

Aknowledgement

This work was supported partly by the Science Research Fund of Ministry of Education and Culture (General Research Category C No. 60550039, 1984-1986), by Drs. T. Ogawa and T. Ishiguro, the Computer Center of National Aerospace Laboratory, Tokyo, and by Profs. H. Oguchi and T. Abe, ISAS (Institute of Space and Astronautical Sciences) regarding AOTV project.

References

1) Rakich, J. V., Bailey, H. E. and Park, C.; Computation of Nonequilibrium, Supersonic Three-dimensional Inviscid Flow over Blunt-Nosed Bodies. AIAA Journal Vol. 21, No. 6, June 1983.
2) Rizzi, A. W. and Bailey, H. E.; Reacting Nonequilibrium Flow around the Space Shuttle Using a Time-Split Method. NASA SP-347, 1975.
3) Reddy, K. V. and Fujiwara, T.; A Hybrid Technique for Hypervelocity Flows of Reentry Vehicle with Real Gas Effects, Memoirs of the Faculty of Engineering, Nagoya University, Vol. 39, No. 2, Oct. 1987.
4) Park, C.; On Convergence of Computation of Chemically Reacting Flows. AIAA Paper No. 85-0247, Jan. 1985.
5) Kuo, K. K.; Principles of Combustion, John Wiley & Sons, 1986.
6) JANAF Thermochemical Tables, NSRDS, 1971.
7) Beam, R. and Warming, R. F.; An Implicit Factored Scheme for the Compressible Navier-Stokes Equations, AIAA Papar No. 77-645, June 1977.
8) Pulliam, T. H.; Artificial Dissipation Models for the Euler Equations, AIAA Paper No. 85-0438, Jan 1985.
9) Pulliam, T. H. and Steger, J. L.; Implicit Finite-Difference Simulation of Three-Dimensional Compressible Flow. AIAA Journal, Vol. 18, No. 2, Feb. 1980.

10) Wang, Y. Y. and Fujiwara, T.; Numerical Analysis of Transonic Flow around a Two-Dimensional Airfoil by Solving Full Navier-Stokes Equations, Memoirs of the Faculty of Engineering, Nagoya University, Vol. 36, No. 2, pp. 138-178, 1984.

Appendix

$\hat{A}^n$, $\hat{B}^n$ and $\hat{C}^n$ in Eq. (25) are the Jacobian matrices obtained in the time linearization of $\hat{E}^n$, $\hat{F}^n$ and $\hat{G}^n$, respectively,

$$\text{i. e.} \quad \hat{A}^n=\frac{\partial \hat{E}^n}{\partial \hat{q}^n},\ \hat{B}^n=\frac{\partial \hat{F}^n}{\partial \hat{q}^n},\ \hat{C}^n=\frac{\partial \hat{G}^n}{\partial \hat{q}^n}.$$

After performing differentiation of each term, $\hat{A}^n$, $\hat{B}^n$ and $\hat{C}^n$ can be obtained as follows:

$\hat{A}$, $\hat{B}$, or $\hat{C}=$

$$\begin{pmatrix}
\theta\left(1-\frac{\rho_1}{\rho}\right)k_0 & -\theta\frac{\rho_1}{\rho} & -\theta\frac{\rho_1}{\rho} & -\theta\frac{\rho_1}{\rho} & -\theta\frac{\rho_1}{\rho} & k_x\frac{\rho_1}{\rho} \\
 & & & k_y\frac{\rho_1}{\rho} & k_z\frac{\rho_1}{\rho} & 0 \\
-\theta\frac{\rho_2}{\rho} & \theta\left(1-\frac{\rho_2}{\rho}\right) & -\theta\frac{\rho_2}{\rho} & -\theta\frac{\rho_2}{\rho} & -\theta\frac{\rho_2}{\rho} & k_x\frac{\rho_2}{\rho} \\
 & & & k_y\frac{\rho_2}{\rho} & k_z\frac{\rho_2}{\rho} & 0 \\
-\theta\frac{\rho_3}{\rho} & -\theta\frac{\rho_3}{\rho} & \theta\left(1-\frac{\rho_3}{\rho}\right) & -\theta\frac{\rho_3}{\rho} & -\theta\frac{\rho_3}{\rho} & k_x\frac{\rho_3}{\rho} \\
 & & & k_y\frac{\rho_3}{\rho} & k_z\frac{\rho_3}{\rho} & 0 \\
-\theta\frac{\rho_4}{\rho} & -\theta\frac{\rho_4}{\rho} & -\theta\frac{\rho_4}{\rho} & \theta\left(1-\frac{\rho_4}{\rho}\right) & -\theta\frac{\rho_4}{\rho} & k_x\frac{\rho_4}{\rho} \\
 & & & k_y\frac{\rho_4}{\rho} & k_z\frac{\rho_4}{\rho} & 0 \\
-\theta\frac{\rho_5}{\rho} & -\theta\frac{\rho_5}{\rho} & -\theta\frac{\rho_5}{\rho} & -\theta\frac{\rho_5}{\rho} & \theta\left(1-\frac{\rho_5}{\rho}\right) & k_x\frac{\rho_5}{\rho} \\
 & & & k_y\frac{\rho_5}{\rho} & k_z\frac{\rho_5}{\rho} & 0 \\
-u\theta+k_x\psi_1 & -u\theta+k_x\psi_2 & -u\theta+k_x\psi_3 & -u\theta+k_x\psi_4 & -u\theta+k_x\psi_5 & \theta+uk_x\left(1+\frac{1}{\varepsilon}\right)+k_0 \\
 & & & k_yu+k_zv & k_zu+k_xw & -\frac{k_x}{\varepsilon} \\
-v\theta+k_y\psi_1 & -v\theta+k_y\psi_2 & -v\theta+k_y\psi_3 & -v\theta+k_y\psi_4 & -v\theta+k_y\psi_5 & k_zv+k_yu \\
 & & & \theta+vk_y\left(1+\frac{1}{\varepsilon}\right)+k_0 & k_zv+k_yw & -\frac{k_y}{\varepsilon} \\
-w\theta+k_z\psi_1 & -w\theta+k_z\psi_2 & -w\theta+k_z\psi_3 & -w\theta+k_z\psi_4 & -w\theta+k_z\psi_5 & k_zw+k_zu \\
 & & & k_yw+k_zv & \theta+wk_z\left(1+\frac{1}{\varepsilon}\right)+k_0 & -\frac{k_z}{\varepsilon} \\
\theta\psi_1-(e+p)\frac{\theta}{\rho}, & \theta\psi_2-(e+p)\frac{\theta}{\rho}, & \theta\psi_3-(e+p)\frac{\theta}{\rho}, & \theta\psi_4-(e+p)\frac{\theta}{\rho}, & \theta\psi_5-(e+p)\frac{\theta}{\rho}, & \frac{k_x}{\rho}(e+p)+\theta\frac{u}{\varepsilon} \\
 & & & \frac{k_y}{\rho}(e+p)+\theta\frac{v}{\varepsilon}, & \frac{k_z}{\rho}(e+p)+\theta\frac{w}{\varepsilon}, & \theta\left(1-\frac{1}{\varepsilon}\right)+k_0
\end{pmatrix}$$

where

$$\theta = k_x u + k_y v + k_z w, \qquad \varepsilon = 1 - \frac{C_p}{\overline{R}}, \qquad \overline{R} = \frac{1}{\rho} \sum_{l=1}^{N} \frac{\rho_l}{\mathrm{M}_l} R_0,$$

$$\psi_i = \frac{1}{\varepsilon} \left[\sum_{l=1}^{N} \frac{\rho_l}{\rho} h_l - \frac{C_p T}{\mathrm{M}_i} \frac{R_0}{\overline{R}} + 0.5 (u^2 + v^2 + w^2) \right].$$

To Obtain $\hat{A}$, set $k_0 = \xi_t$, $k_x = \xi_x$, $k_y = \xi_y$ and $k_z = \zeta_z$.

To Obtain $\hat{B}$, set $k_0 = \eta_t$, $k_x = \eta_x$, $k_y = \eta_y$ and $k_z = \eta_z$.

To Obtain $\hat{C}$, set $k_0 = \zeta_t$, $k_x = \zeta_x$, $k_y = \zeta_y$ and $k_z = \zeta_z$.